Assessment of Upper-Extremity Joint Angles Using Harmony Exoskeleton

Ana C. De Oliveira, James S. Sulzer, and Ashish D. Deshpande

***Abstract*— The biomechanical complexity of the human shoulder, while critical for functionality, poses a challenge for objective assessment during sensorimotor rehabilitation. With built-in sensing capabilities, robotic exoskeletons have the potential to serve as tools for both intervention and assessment. The bilateral upper-extremity Harmony exoskeleton is capable of full shoulder articulation, forearm flexion-extension, and wrist pronation-supination motions. The goal of this paper is to characterize Harmony's anatomical joint angle tracking accuracy towards its use as an assessment tool. We evaluated the agreement between anatomical joint angles estimated from the robot's sensor data and optical motion capture markers attached to the human user. In 9 healthy participants we examined 6 upper-extremity joint angles, including shoulder girdle angles, across 4 different motions, varying active/passive motion of the user and physical constraint of the trunk. We observed mostly good to excellent levels of agreement between measurement systems with $CMC_{ip} > 0.65$ for shoulder and distal joints, magnitudes of average discrepancies varying from 0.43° to 16.03° and width of LoAs ranging between 9.44° and 41.91°. Slopes were between 1.03 and 1.43 with $r > 0.9$ for shoulder and distal joints. Regression analysis suggested that discrepancies observed between measured robot and human motions were primarily due to relative motion associated with soft tissue deformation. The results suggest that the Harmony exoskeleton is capable of providing accurate measurements of arm and shoulder joint kinematics. These findings may lead to robot-assisted assessment and intervention of one of the most complex joint structures in the human body.**

***Index Terms*— Rehabilitation robotics, exoskeletons, kinematics, assessment.**

I. Introduction

STROKE is the leading cause of long-term disability in the United States [1] and in the past few decades a number of interventions have been adopted for rehabilitation of patients with upper-extremity motor impairments [2]. Monitoring changes in the upper-extremity kinematics is critical for determining the most effective interventions for a particular patient and condition [3], [4]. Conventional methods for assessment of function and impairment are inherently subjective [5]–[7]. More objective methods for kinematics assessment such as goniometers and inclinometers are limited to certain joints, suffer from inaccuracy [8], and are time consuming. Motion capture (mocap) systems are generally accurate and reliable, but their use is time consuming, costly, and impractical, primarily limiting them to research labs. Robotic exoskeletons have emerged as a potential alternative intervention for upper-extremity rehabilitation [9]–[12]. Due to their built-in sensing capabilities that provide high-resolution, robust, and consistent measurements of kinematic and kinetic quantities, exoskeletons create an exciting possibility for assessing movement behavior simultaneously with delivering therapy.

The critical yet intricate shoulder complex has been a challenge to objectively assess and manipulate for therapists. The shoulder is composed of several joints including a floating joint of the scapula, connected to the clavicle and humerus through soft tissue. Altogether the shoulder could be modeled as being composed of five degrees-of-freedom (DoFs). The coordination between the scapula and humerus, known as the scapulohumeral rhythm (SHR) [13], is often impaired in shoulder dysfunction [14], [15]. A few attempts have been made to actively assist shoulder movements with robotic devices to treat impairments [16]–[21]. However, all these systems introduce some form of simplification around the patient's shoulder complex. To ensure accuracy of measured anatomical parameters it must be assumed that robotic exoskeletons i) are sufficient and capable of tracking the user's movements and inferring anatomical joint angles and ii) do not interfere with the user's natural movements in a significant way. The simplification of the robot structure may induce unintended reaction forces and over-constrain motions. Further, the compliance of the physical interface between the human and robot [22] can result in intractable relative movements between user and robot. Thus, to be an effective assessment tool, a robotic exoskeleton must be capable of accommodating motions at the level of complexity of the joint while limiting the interface compliance to avoid excessive relative motions.

We have developed an exoskeleton for bilateral upper-extremity rehabilitation called Harmony (Fig. 1) [23]. The shoulder mechanism in Harmony has been designed to actively support the full mobility of the shoulder in all 5 DoFs allowing natural movements [24]. However, the accuracy of Harmony in assessment of the user's joint kinematics has not been evaluated. In this paper we carry out a quantitative comparison of kinematic assessment with Harmony exoskeleton and an optical mocap system. We focus on anatomical joint-space parameters important for assessment of shoulder movements. This work may lead to clinically relevant assessments in

Manuscript received September 21, 2020; revised March 9, 2021; accepted April 11, 2021. Date of publication April 19, 2021; date of current version May 19, 2021. This work was supported in part by the National Science Foundation (NSF) under Grant 2019704 and in part by the Coordenação de Aperfeiçoamento de Pessoal de Nível Superior - Brasil (CAPES) - Finance Code 001. *(Corresponding author: Ashish D. Deshpande.)*

This work involved human subjects or animals in its research. Approval of all ethical and experimental procedures and protocols was granted by the Internal Review Board organized by the Office of Research Support in The University of Texas at Austin under Protocol No. 2013-05-0126 approved on July 18, 2019.

The authors are with the Walker Department of Mechanical Engineering, The University of Texas at Austin, Austin, TX 78712 USA (e-mail: ashish@austin.utexas.edu).

Digital Object Identifier 10.1109/TNSRE.2021.3074101

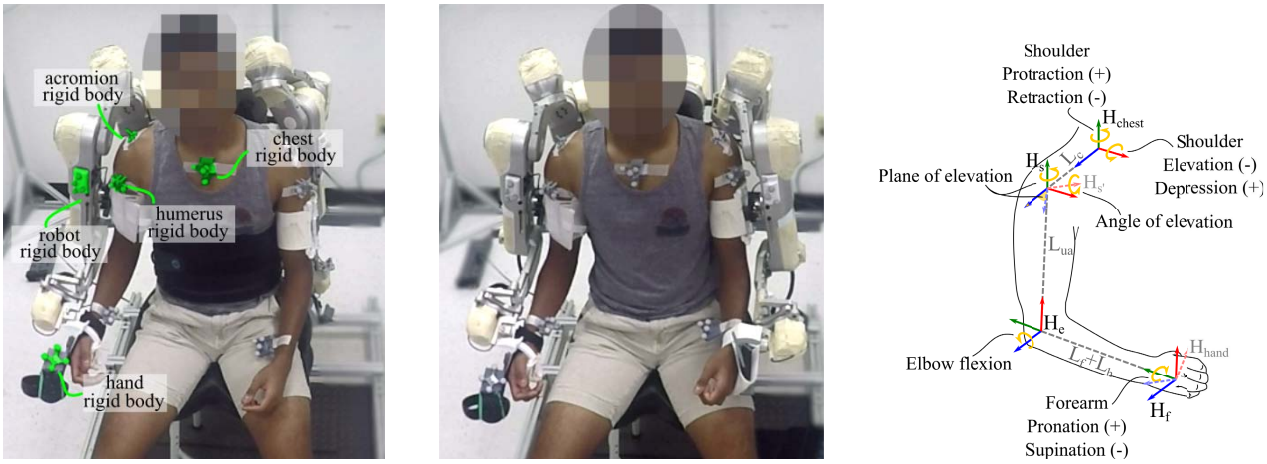

(a) (b) (c)

Fig. 1. Experimental protocol illustration. Marker placement is shown in (a), where the markers grouped in rigid-bodies were highlighted in green (rigid bodies not highlighted were not used in this study). Different trunk-restraint methods adopted in the active conditions of the experimental protocol are shown in (a) and (b). Active-abdominal condition is represented in (a), where the trunk is constrained with a belt wrapped around the abdomen, and active-bilateral condition is represented in (b), where the trunk is constrained with a bilateral attachment to the robot. The kinematic model used to represent anatomical parameters of the human arm is depicted in (c). Acronyms L_c, L_{ua}, L_f, and L_h represent the lengths of clavicle, upper-arm, forearm, and hand, respectively. In the picture, the participant was positioned in the calibration pose, with σ, SE, SP, SAE, and FPS at 0° (SPE singular) and EF at 90°.

TABLE I
DEFINITION OF ISB COORDINATE FRAMES

Frame	Transformation
H_s	$H_{chest}R_{(x,SE)}R_{(y,SP)}T_{(z,L_c)}$
$H_{s'}$	$H_sR_{(y,SPE)}R_{(x,SAE)}$
H_e	$H_sR_{(y,\sigma)}T_{(y,-L_{ua})}$
H_f	$H_eR_{(z,EF)}T_{(y,-L_f-L_h)}$
H_{hand}	$H_fR_{(y,FPS)}$

SE and SP: shoulder elevation-depression and protraction-retraction
SPE and SAE: shoulder plane and angle of elevation
EF: elbow flexion, FPS: forearm pronation-supination

post-stroke patients that often exhibit disrupted inter-joint coordination [25].

II. Materials and Methods

A. Modeling

To extract anatomical joint angles, we defined coordinate systems located at the center-of-rotation (CoR) of each joint, following the recommendations from the International Society of Biomechanics (ISB) [26]. Based on Harmony's active DoFs we analyzed the following six anatomical joint angles: shoulder elevation-depression, shoulder protraction-retraction, shoulder angle of elevation, shoulder plane of elevation, elbow flexion, and forearm pronation-supination. We show the transformations used to define the ISB coordinate systems as a function of the anatomical joint angles in Table I and illustrate it in Fig. 1c. The symbols H_A, $R_{(k,a)}$, and $T_{(k,a)}$ represent a coordinate system A in the inertial frame, a rotation of α around the k-axis, and a translation of a in k, respectively. The quantity σ is the angle between the z-axis of H_s and the axis-of-rotation of the elbow joint represented in the inertial frame.

We adopted an optical mocap system with passive markers as the benchmark sensing modality. We grouped markers into rigid bodies that allow tracking of position and orientation (Fig. 1). We adjusted markers and camera placement to overcome constraints and limitations of the environment, particularly the occlusions and limited access to specific body segments introduced by the robot (Fig. 1a). We anticipated to observe relative movement of the human limb with respect to the robot and to quantify this movement we placed a rigid body on the robot's upper-arm linkage. Since the elbow and hand could not be directly tracked due to occlusion constraints, we chose to track the upper-arm and the interface attached to the hand, assuming that there is no significant relative movement with respect to the hand. This is a reasonable assumption, given that the custom-made interface used in the experiments constrains the hand and wrist in three locations, limiting the relative motion at the wrist joint. To calculate the desired joint angles, we must track axis of rotation (AoR) of both the elbow and forearm. To obtain these parameters from the available rigid bodies, we adopted a least-squares algorithm [27] that uses data captured during isolated elbow flexion-extension and forearm pronation-supination movements. It gives a relationship between the humerus rigid body and elbow AoR, and between the hand rigid body and forearm AoR.

To define coordinate systems from mocap data representing the kinematic model of the human arm, we used a priori information about the user's configuration to define the CoR of each joint. This information consists of a known calibration pose and the measured user's arm segments between the bony landmarks: manubrium, acromion process, lateral epicondyle, and ulnar styloid process. The coordinate systems, angles, and calibration pose are depicted in Fig. 1c. We averaged rigid body data captured over a 10 second window during the calibration pose, and used it to calculate rigid transformations from the tracked rigid bodies to the defined ISB coordinate systems. H_{chest} was defined by the chest rigid body, and shoulder, elbow, and forearm CoRs were defined by the acromion, humerus, and hand rigid bodies. These rigid transformations were then further applied to estimate anatomical joint angles from tracked rigid bodies for any arbitrary movement.

Harmony exoskeleton is equipped with position encoders attached axially to each of the robot's 14 DoFs (seven on each side). The robot's structure was modeled as a kinematic

TABLE II
DENAVIT-HARTENBERG PARAMETERS REPRESENTING HARMONY

Joint	a	α	d	θ
1	L_c	$-90°$	0	θ_1^*
2	0	0	0	θ_2^*
2′	0	$90°$	0	$-\theta_2^*$
3	0	$-60°$	0	$\theta_3^* + 35.3°$
4	0	$60°$	0	$\theta_4^* - 109.5°$
5	L_{ua}	0	0	$\theta_5^* + 125.3°$
6	0	0	0	$\theta_6^* - 90°$
6′	0	$90°$	0	0
7	0	0	$L_f + L_h$	θ_7^*

chain with nine DoFs, seven active and two dummy joints to accommodate the 4-bar-mechanism structure of the shoulder and to adjust the end-point frame. This kinematic chain can be represented using the Denavit-Hartenberg parameters in Table II [23], [28]. Symbols θ_i^* represents a variable angle for a joint i. The coordinate system of each joint can be obtained from measured joint angles using forward kinematics [28]. Because the coordinate systems resulting from this model differ from the ISB recommendation in Fig. 1c, we defined a second model based on the same principles used for the mocap data to obtain a comparable structure. During the calibration pose, we averaged angles measured by the robot sensors over the same 10 second window and calculated rigid transformations from the robot's kinematic chain coordinate systems to the ISB coordinate systems. H_{chest} was defined by the robot's inertial frame, and shoulder, elbow, and forearm CoRs were defined by the coordinate systems attached to joints 4, 5, 6′, and 7. These transformations were then further applied to estimate anatomical joint angles from the robot's sensor data for any arbitrary movement.

The adopted calibration pose was defined beforehand and programmed into Harmony. During the calibration procedure, the robot drove a participant's arm to the calibration pose and locked its position. The robot's configuration for calibration was manually defined by physically aligning the upper-arm and forearm linkages perpendicular and parallel to the ground, respectively, using a level measuring tool. We positioned the remaining joints such that the end-effector pointed approximately forward with respect to the robot's inertial frame.

B. Experimental Protocol

The goal of the experiments was to quantify discrepancies between joint angles estimated by robot's sensors and mocap data during four single DoF movements: shoulder flexion-extension, shoulder horizontal abduction-adduction, elbow flexion-extension, and forearm axial rotation. These movements were used to evaluate shoulder angle of elevation, shoulder plane of elevation, elbow flexion, and forearm pronation-supination, respectively. Shoulder-girdle angles in Harmony are a result of the SHR assistance and not actively driven by the user. Therefore, shoulder elevation-depression and protraction-retraction were evaluated from shoulder flexion-extension and horizontal abduction-adduction respectively, where the angles' ranges of motion (ROM) were significant.

Patients with motor impairments, particularly stroke patients, exhibit compensation for arm impairment by rocking or swinging their trunk [29]. To encourage arm motion some form of trunk restraint must be used. With Harmony two possible solutions exist for restraining the trunk: either using an abdominal harness that allows for free arm movement or attaching both of the patient's arms to the bilateral robot. To study assessment performance under all possible methods of movement execution and trunk restraint, each movement was performed under three different conditions: (i) *passive*: the robot drives the movement while user is passive (eight repetitions), (ii) *active-abdominal*: user drives the movement with trunk constrained by an abdominal belt that attaches to the robot's structure (seven repetitions), and (iii) *active-bilateral*: user drives the movement; there is no abdominal constraint but the left arm is attached to the robot in a stationary position (seven repetitions). The two active conditions are illustrated in Figs. 1a and 1b. A baseline control implemented in Harmony [23] compensates for its dynamics to ensure transparency for the user (i.e., require minimal forces to move the robot) in the active conditions, and an impedance controller enables full assistance in the passive condition.

In the active conditions participants received visual feedback of their current joint angle and target at all times. To avoid biasing the results, real-time feedback was acquired with the Oculus Touch Controller (Oculus VR, Menlo Park, CA, USA) attached to the hand interface. To ensure consistency of task execution across participants, we controlled movement speed using visual cues by making consecutive targets active or inactive, and auditory cues consisting of beeps from a metronome following the desired speed. We adjusted the metronome to match the speed in which the robot executed the motion in the passive condition. Since we wanted to replicate the same ROM in all experimental conditions, we first programmed the joint trajectories in the robot for the passive condition. In this process, we ensured movements did not result in collisions and occlusions of the rigid bodies with body parts, limited movements to be within the robot's ranges, and ensured the Oculus Touch Controller was within the field of view of its tracking system. Since the robot's DoFs in the shoulder do not exactly match an anatomical shoulder's DoFs, the joint trajectories for the single DoF movements were determined with a teach-and-play methodology. The ranges of motion defined for each movement and joint were: In shoulder flexion-extension, shoulder angle of elevation varied from $-40°$ to $-90°$ in the $90°$ shoulder plane of elevation, with elbow flexion and forearm pronation-supination in $0°$. In shoulder horizontal abduction-adduction, shoulder plane of elevation varied from $60°$ to $100°$ in the $-90°$ shoulder angle of elevation, with elbow flexion and forearm pronation-supination in $0°$. In elbow flexion-extension, elbow flexion varied from $50°$ to $120°$, with shoulder angle of elevation, shoulder plane of elevation, and forearm pronation-supination in $0°$. In forearm axial rotation, forearm pronation-supination varied from $-45°$ to $45°$, with shoulder angle of elevation and shoulder plane of elevation in $0°$, and elbow flexion in $90°$.

We instructed participants to start from the indicated initial position, moving to the opposite extreme and back to the start for as many times as required, following the visual and auditory cues and attempting to achieve a movement as smooth as possible. All of the movements were executed with the right

arm, and participants practiced all movements outside of the robot to get familiarized with the speed and range. During data acquisition, they performed eight back-to-back repetitions in the passive condition and seven in both active conditions (active-abdominal, and active-bilateral).

Harmony's interfaces are detachable, which facilitates consistent arm and shoulder locations with respect to the robot across dons and doffs. To also maximize consistency across participants we attached the hand and upper-arm interfaces outside of the robot before the experiment started. The hand interface requires a specific hand placement to grip the hand thenar and hypothenar eminences along with the wrist, which reduces its placement variability. The upper-arm interface was attached with its lower edge 7.15 cm away from the lateral epicondyle, which is the distance between the robot's elbow joint axis and the lower edge of the interface's cuff. Upper-arm circumference varies across subjects, and to accommodate this variability the cuff was secured in place with a fabric strap and Velcro. To control its tightness, we used a force sensitive resistor (FlexiForce™) embedded to the cuff's structure, and we adjusted the tightness pulling the strap to reach 0.3N.

C. Participants

The target population for this study was right-handed able-bodied individuals that had no known shoulder injury and whose body dimensions were within the limits of the Harmony exoskeleton. Nine participants (6M/3F, age 27.8 ± 5.9 [20, 39] years, $L_c = 20.3 \pm 1$ [18.5, 21.5] cm, $L_{ua} = 31.7 \pm 0.8$ [30, 33] cm, and $L_f = 26.3 \pm 1.63$ [24, 28.5] cm), were enrolled and performed the experimental protocol. The experimental procedure was approved by the Internal Review Board organized by the Office of Research Support in The University of Texas at Austin under the protocol number 2013-05-0126 approved on July 18 2019, and the participants provided written informed consent that was reviewed by the board.

D. Data Acquisition and Analysis

We tracked mocap data with the Optitrack Prime 17W system (NaturalPoint Inc., Corvallis, OR, USA) using 10 cameras with a sampling rate of 120 fps, and manually checked for labeling errors and missed data-points. We securely attached rigid bodies to the participants' skin with tape on the sternum (right below the jugular notch), acromion, and above the biceps brachii (Fig. 1a). We also fixed one rigid body to the hand interface and another to the robot's upper-arm linkage. There were no observations of rigid bodies missing all of their markers for more than a few milliseconds, and we performed interpolation using cubic splines followed by a pattern-based interpolation algorithm as necessary. We used a fourth-order low pass Butterworth filter with a cut-off frequency of 2 Hz to filter tracked positions of all markers before solving for the rigid bodies. We tracked robot joint angles with built-in high-resolution magnetic rotary encoders (Contelec AG Inc.) with a sampling rate of 100 Hz, and filtered the data using a fourth-order low-pass Butterworth filter with a cut-off frequency of 10 Hz. Different cut-off frequencies were selected to obtain similar noise properties. We synchronized mocap and robot sensor data via threshold velocity of the measured joint in each motion, matching the initial time of the two data sets when the velocity magnitude exceeded 5 deg/s.

We distinguished repetitions with peak identification using mocap data to determine the initial time instant and duration of each repetition. We trimmed the time-series datasets and normalized their times between 0 and 100% of both mocap and robot data. To obtain AoR of the elbow and forearm, we adopted a least-squares algorithm [27] that uses data captured during isolated elbow flexion-extension and forearm pronation-supination movements. For that purpose we used the first two repetitions in the passive condition of these two movements, which were excluded from the agreement analysis in the passive condition. Furthermore, we also excluded from the analysis the last repetition in the passive condition to eliminate transitioning effects. Regarding the active conditions, we excluded the first and last repetitions from the analysis to eliminate transitioning effects.

We used Bland-Altman plots [30] to qualitatively evaluate the angle agreement between robot and mocap. These plots indicate an average error along with limits of agreement (LoA). The LoA indicate a region within which one should expect the discrepancy to fall. If a linear trend is present in these plots, it indicates a relationship between discrepancy and joint angle, in which case the LoA becomes conservative. We used a repeated measures correlation (rmcorr) [31] analysis to estimate linear models relating robot and mocap angles with subject-specific intercepts. We adopted LoA and overall slope from the rmcorr analysis as primary outcomes to indicate agreement between the robot and mocap. The slope represents proportional bias and a one-to-one relation indicates perfect agreement between mocap and robot data. Slopes parallel to the one-to-one indicate accurate proportional association with a systematic bias, such that negative intercepts imply underestimation by the robot when compared with mocap, whereas positive intercepts imply overestimation. We adopted the coefficient of multiple correlation interprotocol (CMC_{ip}) [32] proposed by Ferrari *et al.* [33] as a metric of reproducibility to quantify the degree of agreement between the two sensing modalities. The CMC_{ip} quantifies the similarity between two waveforms between zero and one by taking into account shape differences, systematic bias, correlation, and ROM. We used all five repetitions of each movement and condition to calculate intra-subject CMC_{ip}. Since values across participants do not follow a normal distribution due to ceiling effects, we calculated the median and interquartile range (IRQ). We interpreted values as excellent ($0.95 < \text{CMC} < 1$), very good ($0.85 < \text{CMC} < 0.95$), good ($0.75 < \text{CMC} < 0.85$), moderate ($0.65 < \text{CMC} < 0.75$), and poor ($0 < \text{CMC} < 0.65$) [34]. It is common to obtain complex CMC_{ip} values for curves with limited ROM and high dispersion and we interpreted these results as dissimilarity [33]. The correlation coefficient (r) derived from the rmcorr analysis and root mean square of the difference (RMSD) were used as supplementary outcomes. The coefficient r evaluates the strength of the association between measurements from mocap and the robot and represents the reliability of

the calculated slope. We interpreted correlation as excellent ($r > 0.9$), good ($0.7 < r < 0.9$), moderate ($0.5 < r < 0.7$), low ($0.3 < r < 0.5$), and negligible ($r < 0.3$) [35]. The RMSD represents the overall discrepancy between the two sensing modalities over the entire movement duration and is a metric traditionally reported in method agreement analysis. We also calculated the minimal detectable change (MDC) as a representation of within-subject measurement sensitivity in each movement and condition. The MDC is given by $1.96 \times \text{SEM} \times \sqrt{2}$ [36] and was derived from mocap data in all five repetitions. SEM is the standard error of measurement given by the root mean of the within-subjects variances, averaged across time. We also evaluated intra-subject repeatability in each condition using the coefficient of multiple correlation within-protocol proposed by Ferrari *et al.* [33] from mocap and robot data, referred to as CMC_m and CMC_r, respectively. They were calculated and interpreted similarly to the CMC_{ip} but only using datasets of their respective sensing modality. High intra-subject repeatability from mocap data suggests that MDC values are likely associated with measurement- rather than performance-variability. The MDC is a baseline to assess if differences between the two measurement modalities fall within an acceptable range. RMSD values lower than the MDC indicate an acceptable discrepancy, since it suggests the inability of the benchmark system to capture the observed differences. To minimize effects of within-subject movement variability, we averaged the five repetitions to obtain one dataset instance of a specific movement and condition for these analyses, with the exception of the MDC and CMC metrics.

To generate Bland-Altman plots and perform rmcorr analysis, data points must be independent of each other. However, time-series datasets do not meet this criterion. To minimize biases introduced by the time-dependency among data points and have a dataset distribution as close to the Gaussian distribution as possible, we resampled both mocap and robot data to obtain 20 data points in each dataset equally spaced in time, totaling 180 data points for each movement and condition. We then visually inspected the datasets as represented in histograms to check for normality, and no significant skewness was observed in any movement or condition. Because of the time-dependency of the samples, the LoA of the Bland-Altman plots were calculated using the standard 95% confidence interval and the non-parametric method described in [37].

To calculate relative movement between the robot and human, we extracted time-series translations and rotations between the robot's and humerus's rigid bodies and the translations between the robot's and acromion's rigid bodies in 3D relative to the robot's rigid body frame. To capture the changes in the humerus configuration, we used the humerus's rigid body to obtain the orientation of the coordinate system attached to the shoulder, and only the position of the acromion's rigid body was applied in the estimation of anatomical joint angles. Therefore, we did not extract relative rotations of the acromion for relative movement analysis. Furthermore, we also calculated movements of the trunk with respect to the calibration pose, as represented by translations and rotations of the rigid body placed on the chest in 3D relative to the chest's rigid body frame in the calibration pose. Therefore, we obtained a total of 15 variables to represent relative movement between human and robot: relative translations in 3D of humerus, chest, and acromion, and relative rotations in 3D of humerus and chest.

III. Results

Table III summarizes the results for the metrics adopted to indicate agreement between angles measured by the robot and mocap. The width of LoAs ranged between 9.44° and 41.91° with magnitudes of average discrepancies varying from 0.43° to 16.03°. The slopes for each joint ranged between 0.47 and 1.65. The RMSD ranged between 2.10°(0.70°) and 15.94°(2.62°). The greatest agreement was in the forearm pronation-supination, which demonstrated narrowest LoAs, all within the range $[-10°, 6°]$, slopes closest to one, all under 1.05, and excellent degrees of agreement indicated by CMC_{ip} values. The greatest discrepancy was in the shoulder protraction-retraction, which demonstrated slopes most distant from one with the lowest correlation coefficients and waveform dissimilarities indicated by complex CMC_{ip} values. The lowest movement variability was observed in the shoulder girdle angles as indicated by MDC values, all under 3.15° and as low as 1.64°. The largest movement variability was in the forearm pronation-supination with MDC values up to 13.29°.

The Bland-Altman plots generated for each joint and condition are shown in Fig. 2. In each of the six figures, each column represents one condition. We depicted the average joint angle trajectory over normalized time and standard deviation calculated across all participants, estimated by both mocap and robot sensor data. We show values of CMC_r and CMC_m for each condition in the bottom of these figures, indicating mostly excellent intra-subject repeatability for the DoFs targeted by the experimental tasks (shoulder plane and angle of elevation, elbow flexion, and forearm pronation-supination) in both sensing modalities. Right below the trajectory, we present the overall (red) and participant-specific slopes as well as the 20 samples per participant used in the analysis. The slopes represented in Table III reflect the visual illustration of the overall slopes shown by the red lines. The one-to-one slope (black dotted line) indicates perfect agreement. The bottom-most figures represent the Bland-Altman plots, with the average discrepancy observed across all participants and the standard and non-parametric LoAs.

Overall, elbow flexion and forearm pronation-supination presented excellent degree of agreement as indicated by CMC_{ip} values. LoAs for elbow flexion and forearm pronation-supination indicate discrepancies falling within a range of approximately $\pm$ 10°, excluding the active-bilateral condition. Slopes are between 1 and 1.1 in all conditions and RMSD values fall under 6.04°(1.83°). Strong agreement of forearm pronation-supination and elbow flexion can also be observed in the time-series data (top rows of Fig. 2) where we can see substantial overlap between the curves.

Results for the shoulder joint angles (shoulder angle and plane of elevation) generally present good to excellent degrees of agreement between robot and mocap estimations, as indicated by the CMC_{ip} values. LoAs are larger compared to

TABLE III
QUANTITATIVE RESULTS FOR THE METRICS USED TO EVALUATE AGREEMENT

Condition	Discrepancy [LoA]	Slope	CMC_{ip} [IQR]	$r_{(170)}$ [CI]	RMSD (SE)	MDC
Shoulder elevation-depression						
passive	1.97° [-6.43°,10.36°]	1.65	–	0.95 [0.93,0.96]	3.45° (0.75)°	3.15°
active-abdominal	1.41° [-6.57°,9.39°]	1.36	–	0.96 [0.95,0.97]	3.21° (0.87)°	2.58°
active-bilateral	2.68° [-5.86°,11.21°]	1.44	–	0.94 [0.92,0.96]	3.89° (0.96)°	2.34°
Shoulder protraction-retraction						
passive	3.59° [-3.15°,10.33°]	0.85	–	0.77 [0.67,0.82]	4.23° (0.88)°	2.62°
active-abdominal	1.52° [-7.16°,10.20°]	0.47	–	0.45 [0.32,0.56]	3.40° (1.08)°	1.64°
active-bilateral	2.80° [-9.53°,15.13°]	0.59	–	0.64 [0.54,0.72]	5.25° (1.54)°	1.73°
Shoulder angle of elevation						
passive	-16.03° [-36.99°,4.92°]	1.43	0.85 [0.65,0.90]	0.99 [0.98,0.99]	15.94° (2.62)°	9.69°
active-abdominal	-4.85° [-16.00°,6.30°]	1.14	0.96 [0.93,0.97]	>0.99	6.27° (1.08)°	7.67°
active-bilateral	-6.32° [-17.61°,4.96°]	1.09	0.94 [0.88,0.97]	>0.99	7.64° (1.01)°	8.90°
Shoulder plane of elevation						
passive	2.90° [-14.60°,20.41°]	1.03	0.96 [0.92,1.00]	>0.99	6.55° (2.30)°	5.67°
active-abdominal	4.15° [-13.16°,21.47°]	1.12	0.90 [0.81,0.98]	>0.99	7.56° (2.06)°	6.14°
active-bilateral	2.21° [-15.26°,19.68°]	1.13	0.95 [0.78,0.97]	>0.99	7.43° (1.71)°	6.51°
Elbow flexion						
passive	0.43° [-6.88°,7.75°]	1.07	>0.99	>0.99	2.31° (0.46)°	3.69°
active-abdominal	-1.88° [-9.31°,5.55°]	1.10	>0.99	>0.99	2.91° (0.69)°	8.12°
active-bilateral	0.73° [-15.60°,17.06°]	1.10	0.98 [0.95,1.00]	>0.99	6.04° (1.83)°	7.70°
Forearm pronation-supination						
passive	-3.91° [-9.02°,1.20°]	1.05	>0.99	>0.99	3.93° (1.31)°	6.51°
active-abdominal	-1.32° [-6.04°,3.40°]	1.04	>0.99	>0.99	2.10° (0.70)°	10.00°
active-bilateral	-2.41° [-9.88°,5.06°]	1.03	>0.99	>0.99	3.65° (1.22)°	13.29°

CI: 95% Confidence Interval, SE: Standard Error, IQR: Interquartile Range (25^{th} to 75^{th} percentile), df: error degrees of freedom, $r_{(df)}$: Correlation coefficient (rmcorr). Missing CMC values indicate complex number.

distal DoFs, but slope values are generally comparable to forearm pronation-supination and elbow flexion (Table III) and Bland-Altman plots (Fig. 2). However, we observed greater discrepancies in the passive condition of shoulder angle of elevation, which shows instances with moderate degree of agreement, as indicated by the CMC_{ip} IQR. This is also reflected in terms of a wider LoA and slope distant from one as well as the time-series data. The shoulder girdle angles showed high discrepancies, with complex CMC_{ip} values suggesting waveforms dissimilarity, and also demonstrated by large LoAs, slopes far from one, and high dispersion of time-series data.

The observed discrepancies particularly in the shoulder angles, motivated a post-hoc analysis to investigate the association of the discrepancies with relative movements between the robot and user. To evaluate the contribution of this relative movement to the observed discrepancies, we fit a linear model considering these discrepancies as an output and the extracted 3D relative translations and rotations of the humerus, acromion, and chest as inputs or predictors. Since we do not have prior knowledge of the inter-correlation between the inputs and their association with the output, we adopted a step-wise regression framework to obtain a model that minimizes errors and redundancies. In this framework, predictors are iteratively evaluated and, starting from zero, added to the model if they significantly contribute to the output's variability indicated by the R^2. We chose to only add elements that increase the R^2 by at least 0.001. Even though we placed markers following a protocol, placement differences across participants are unavoidable. Furthermore, the reactive forces that lead to relative movements change for different motions and conditions, particularly between passive and active performances. Therefore, we ran the step-wise regression for each participant, motion, and condition, and we present the evolution of the R^2 of each resulting model as a function of the predictors in Fig. 3. This result shows that almost 100% of the output variability is related to the inputs variability.

Mocap markers are placed on deformable skin resulting in a source of error [38]. For instance, the humerus's rigid body was placed between the deltoid and biceps, and contraction of these muscles likely resulted in soft-tissue deformations in the upper-arm. These types of deformations could explain the association between relative movement of the humerus and discrepancies in elbow flexion and forearm pronation-supination. The shoulder joint and humerus are part of the same kinematic link; therefore, distance variations between the acromion's and humerus's rigid body imply relative translation between two components of the same kinematic link. This translation could be caused by deformations of the rigid bodies, weak adhesion to the skin, or soft-tissue deformation, all common challenges encountered in mocap marker placement. We will use the term artifacts to describe all the possible causes for the relative translation between the acromion's and humerus's rigid bodies. To evaluate the contribution of these artifacts to the total relative movement, we ran a linear regression to fit a model that takes distance variation between the acromion's and humerus's rigid bodies as covariates and distance variation between the humerus's and robot's rigid bodies as the dependent variable. After visually inspecting the data, we concluded that this relationship can be fit to a quadratic curve. We obtained a model for each movement and condition, and the resulting fit (R^2) of each case are depicted in Fig. 4. Since body features and marker placement vary across participants, the amount of artifacts, and consequently, the effect on the total relative movement, is expected to vary across participants.

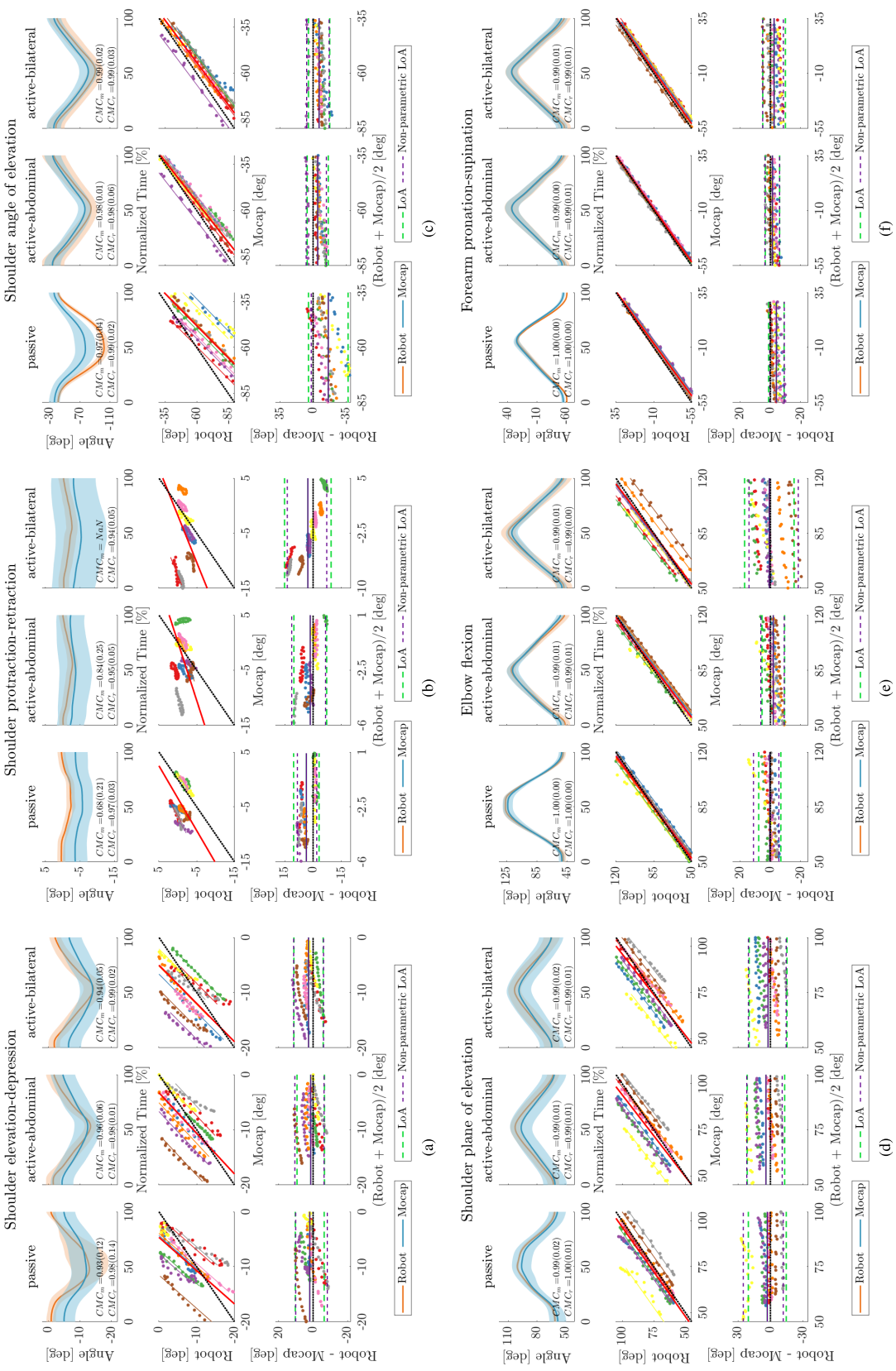

Fig. 2. Relative agreement between robot and mocap using time-series, linear correlation, and Bland-Altman plots. The time series curve averaged across all participants is shown on the top row of each figure, with the shaded area representing the standard deviation. Intra-subject repeatability is represented by the median and interquartile range of CMC_r and CMC_m. The linear correlation is represented in the middle row of each figure. The overall slope is shown in red, and perfect agreement is shown in black for comparison. The Bland-Altman plots are shown in the bottom row of each figure. The average error is represented by a solid purple line, and the zero error is represented by a black dotted line for comparison. LoA and non-parametric LoA are represented by dotted lines. The dots in the middle and bottom rows represent data points, and each color refers to a different participant (nine total).

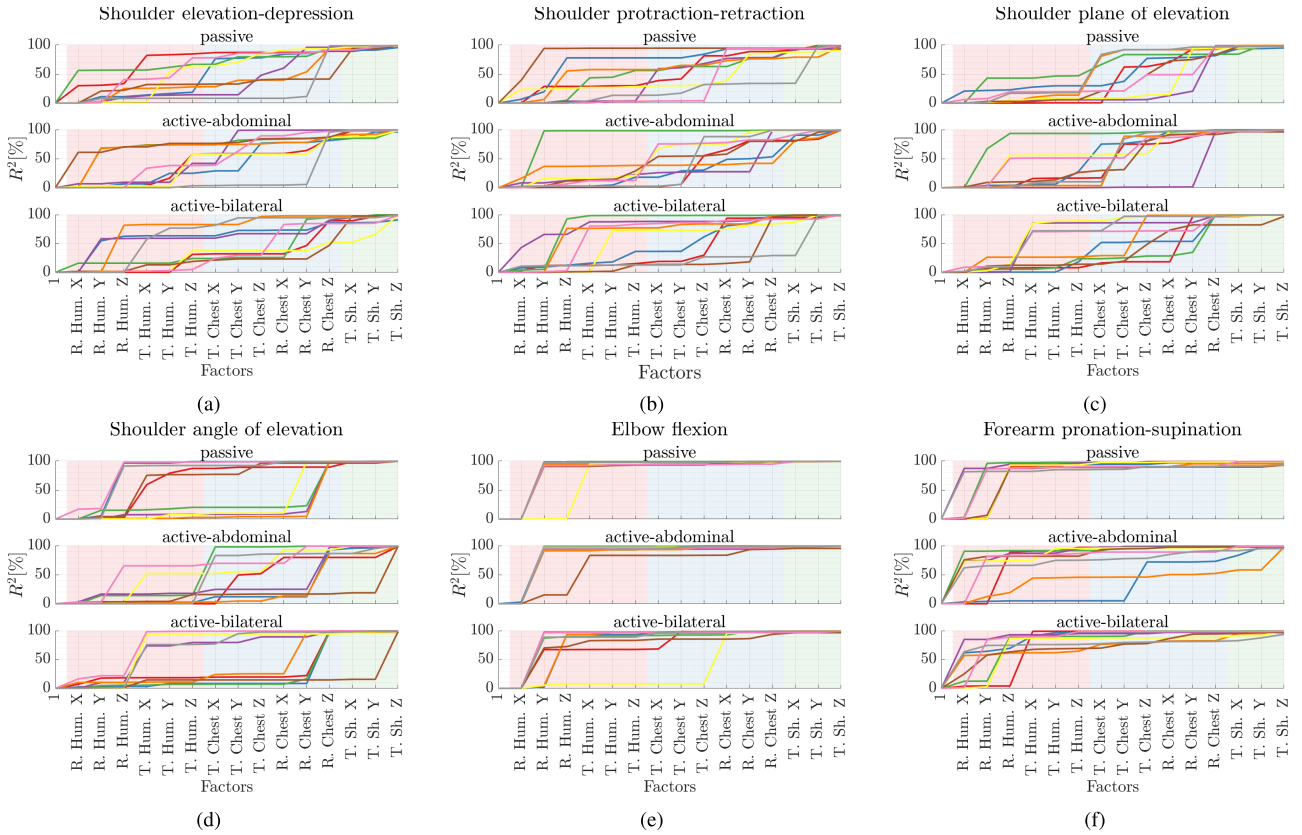

Fig. 3. Association between relative movement and angle discrepancies represented by variance accounted for (R^2). Results for shoulder elevation-depression, protraction-retraction, shoulder plane and angle of elevation, elbow flexion, and forearm pronation-supination are shown in (a)-(f), respectively. Shaded areas separate relative movement in the humerus (red), chest (blue), and shoulder (green). Curves represent the change in R^2 with the addition of each predictor in the linear model. Curves are associated with a single participant and each color refers to a different participant (nine total), and each row represents one condition. The condition "1" represents a linear function consisting of just a constant value.

IV. Discussion

We characterized agreement between kinematic estimations using robot sensor and mocap data and we found excellent degree of agreement ($CMC_{ip} > 0.95$) between robot and mocap estimations of forearm pronation-supination and elbow flexion. We found good to excellent degrees of agreement ($CMC_{ip} > 0.85$) in the shoulder angle and plane of elevation estimations, with the exception of the passive condition in shoulder angle of elevation that exhibited instances of moderate degree of agreement ($0.65 < CMC_{ip} < 0.75$). Finally, results fail to show agreement in the shoulder elevation-depression and protraction-retraction estimations, which exhibited complex CMC_{ip} values likely associated with the limited ROM and high dispersion. We did not observe clear differences between the two types of trunk restraint used in the experiments (active-abdominal and active-bilateral cases).

We found excellent positive correlation ($r > 0.9$) between Harmony's estimation of upper-extremity motions to mocap estimations for most cases, suggesting good reliability of the calculated slope values. Values of CMC_m and CMC_r for the four DoFs targeted by the experimental tasks indicate excellent (>0.95) intra-subject repeatability. This suggests that MDC values are likely associated with measurement- rather than performance- variability. CMC_r also exhibits very good to excellent (>0.85) repeatability for shoulder girdle angles.

During the experiments the participant's arm is attached to the robot at upper-arm and forearm, resulting in a reliable force transmission to the elbow and wrist. Therefore, we expected a high degree of agreement in elbow flexion and forearm pronation-supination. That was indicated by CMC_{ip} values and confirmed by average discrepancies and RMSD values, all falling under the MDCs, narrower LoAs with a total range of approximately 15°, and slopes close to one as shown in Table III. However, we observed higher discrepancies in elbow flexion estimation in the active-bilateral condition (depicted in Fig. 2e). The Bland-Altman plot reveals a constant discrepancy offset that varies across participants, and this resulted in larger LoA and RMSD values. Although LoAs are larger than MDCs in most cases, these limits are conservative in the presence of a linear trend between discrepancy and average angle, which could be confirmed in most cases in Fig. 2.

Given the complexity of the shoulder joint and the indirect force transmission, we expected a lower degree of agreement between robot and mocap in shoulder angle and plane of elevation. Systematic biases are consistently present in both of these angles as shown in Figs. 2c and 2d. This resulted in LoAs and RMSD values that are both larger than the movement variability represented by the MDCs. In this case, LoAs are highly influenced by the different biases demonstrated by each subject as observed in Fig. 2. On the other hand, slopes were close to one with excellent positive correlation ($r > 0.9$). Therefore we concluded that while the shoulder angles estimated by the robot demonstrate low accuracy in absolute terms, the accurate proportional association indicates the ability to capture differential quantities such as velocity. This suggests that although the robot's responsiveness is com-

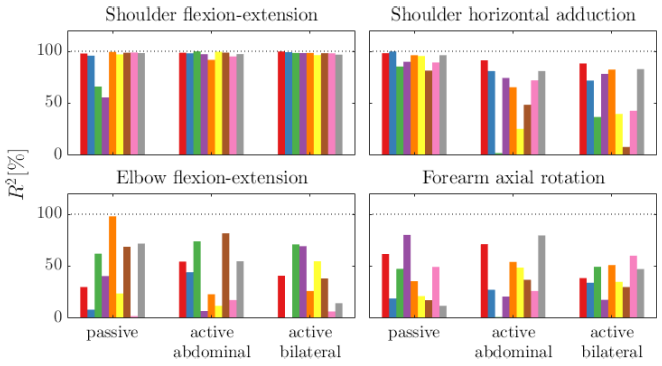

Fig. 4. Association between artifacts and relative movement of the humerus represented by R^2. Each bar represents one participant in a specific condition and each color refers to a different participant (nine total).

parable to mocap's for shoulder angles, estimated angles might not accurately match absolute values of mocap's estimations.

The post-hoc relative movement analysis revealed high association between relative movement (as represented by relative translations and rotations of the humerus, acromion, and chest) and discrepancies, as shown in Fig. 3. An interesting observation in Fig. 3 is that discrepancies in shoulder elevation-depression, protraction-retraction, angle and plane of elevation were associated with chest and humerus relative movement. Discrepancies in elbow flexion and forearm pronation-supination were almost exclusively associated with humerus relative movement. This was somewhat unexpected, since participants were instructed to maintain a static trunk and upper-arm posture during elbow flexion-extension and forearm axial rotation.

We performed post-hoc analysis of the association between artifacts and relative movements to investigate if the unexpected discrepancies could be associated with rigid body deformation, soft-tissue deformation, or weak marker adhesion to the skin. We found high association between our artifact metric and relative motion in the shoulder flexion-extension and horizontal abduction-adduction movements. We found a lower association with elbow flexion-extension and forearm axial rotation movements. This is consistent with previously reported results in the literature indicating that soft tissue artifact is one of the major problems in the use of mocap for the study of upper-extremity motion [38].

The high association between relative movement and estimation discrepancies suggest that we need to constrain the user's movement in the robot. However, this must be balanced with other important factors such as comfort, allowance of natural motion, safety, and ease of don-doff. Furthermore, the association between artifacts and relative movement suggests that even the benchmark sensing modality has limitations and may not be considered as a "ground truth" when evaluating accuracy of exoskeleton devices. The use of bone implants would solve this impasse, but is a challenging method to apply to in vivo human-subject experimental procedures to investigate active movements. A possible compromise would be the combination of the two measurement systems in a Bayesian estimation method such as the Kalman Filter, which uses prior knowledge of the system's dynamics to estimate its state and robust to the inherent measurement uncertainty [39].

Based on the reported results, Harmony is an accurate tool to measure elbow flexion and forearm pronation-supination. It is as sensitive as mocap for the measurement of changes in shoulder angles, but it exhibits offsets that may be associated with the limitations in the mocap system. Further studies are needed to verify if the offsets are caused by untractable relative movements or mocap artifacts. Finally, Harmony is capable of providing estimations of shoulder girdle angles (shoulder elevation-depression and protraction-retraction) which is a novel feature of this rehabilitation robot. However, as compared to mocap the accuracy of the kinematic estimations is low and the variability is high, both of which might be associated with undesirable relative movements. Further research is necessary to investigate if this can be improved with a better trunk constraint. Goniometers are traditionally adopted to measure joint angles in clinical practice. Reliability studies have reported MDC for goniometers varying between 8.3° and 19.4° for forearm pronation-supination [40], between 5.5° and 13.9° for elbow flexion [40], and between 3° and 14° for shoulder flexion [41]. The LoAs reported in this study are comparable with goniometry MDC values for distal joints, which suggests that Harmony's measurement discrepancy with respect to mocap for elbow and forearm angles is within acceptable ranges for clinical practice. However, discrepancy for shoulder angles are larger than the acceptable ranges. This can be attributed in the most part to systematic differences that might be associated with limitations of the adopted benchmark modality. In spite of large shoulder angles discrepancy, Harmony offers the advantage of continuously measuring multiple DoFs during dynamic tasks.

The accuracy observed for Harmony cannot be generalized for all upper-extremity exoskeletons, but the discrepancies observed suggest that similar comparisons should be followed to characterize their accuracy. Although some studies rely on the robot's anatomical measurements [42], such an analysis is under-represented in the literature, and is mostly limited to the forearm and wrist [43]. Attempts to predict established clinical outcomes with anatomical joint angles [42] have found low correlation with shoulder angles, which could be related to low measurement accuracy.

V. Conclusion

The goal of this work was to characterize the Harmony exoskeleton's ability to accurately measure anatomical joint angles, specifically shoulder girdle angles (elevation-depression and protraction-retraction), shoulder angles (angle and plane of elevation), elbow flexion, and forearm pronation-supination. We evaluated the agreement between upper-extremity joint angles estimated from the robot's sensor data and mocap data. The results confirm that the Harmony exoskeleton is capable of providing accurate measurements of arm and shoulder angles given a properly constrained trunk and a well-adjusted, reasonably rigid interface. This establishes the basis to use robotic exoskeletons not only as a tool to deliver therapy, but also to reliably monitor progress, potentially increasing treatment efficiency.

REFERENCES

[1] D. Mozaffarian *et al.*, "Executive summary: Heart disease and stroke statistics-2016 update: A report from the American Heart Association," *Circulation*, vol. 133, no. 4, pp. 447–454, 2016.

[2] C. J. Winstein *et al.*, "Guidelines for adult stroke rehabilitation and recovery," *Stroke*, vol. 47, no. 6, pp. e98–e169, Jun. 2016.

[3] D. U. Jette, J. Halbert, C. Iverson, E. Miceli, and P. Shah, "Use of standardized outcome measures in physical therapist practice: Perceptions and applications," *Phys. Therapy*, vol. 89, no. 2, pp. 125–135, 2009.

[4] C. E. Lang, M. D. Bland, R. R. Bailey, S. Y. Schaefer, and R. L. Birkenmeier, "Assessment of upper extremity impairment, function, and activity after stroke: Foundations for clinical decision making," *J. Hand Therapy*, vol. 26, no. 2, pp. 104–115, Apr. 2013.

[5] L. Santisteban, M. Térémetz, J. P. Bleton, J. C. Baron, M. A. Maier, and P. G. Lindberg, "Upper limb outcome measures used in stroke rehabilitation studies: A systematic literature review," *PLoS ONE*, vol. 11, no. 5, 2016, Art. no. e0154792.

[6] D. J. Gladstone, C. J. Danells, and S. E. Black, "The Fugl-Meyer assessment of motor recovery after stroke: A critical review of its measurement properties," *Neurorehabil. Neural Repair*, vol. 16, no. 3, pp. 232–240, Sep. 2002.

[7] J. Sanford, J. Moreland, L. R. Swanson, P. W. Stratford, and C. Gowland, "Reliability of the Fugl-Meyer assessment for testing motor performance in patients following stroke," *Phys. Therapy*, vol. 73, no. 7, pp. 447–454, 1993.

[8] A. D. Armstrong, J. C. MacDermid, S. Chinchalkar, R. S. Stevens, and G. J. King, "Reliability of range-of-motion measurement in the elbow and forearm," *J. Shoulder Elbow Surgery*, vol. 7, no. 6, pp. 573–580, 1998.

[9] J. Mehrholz, M. Pohl, T. Platz, J. Kugler, and B. Elsner, "Electromechanical and robot-assisted arm training for improving activities of daily living, arm function, and arm muscle strength after stroke," *Cochrane Database Systematic Rev.*, vol. 9, no. CD006876, pp. 1–133, 2018.

[10] R. A. R. C. Gopura, D. S. V. Bandara, K. Kiguchi, and G. K. I. Mann, "Developments in hardware systems of active upper-limb exoskeleton robots: A review," *Robot. Auton. Syst.*, vol. 75, pp. 203–220, Jan. 2016.

[11] Hocoma. *ArmeoPower*. Accessed: Feb. 24, 2021. [Online]. Available: https://www.hocoma.com/solutions/armeo-power/

[12] Kinetec. *ALEx*. Accessed: Feb. 24, 2021. [Online]. Available: http://www.wearable-robotics.com/kinetek/products/alex/

[13] V. T. Inman, J. B. D. M. Saunders, and L. C. Abbott, "Observations on the function of the shoulder joint," *J. Bone Joint Surgery*, vol. 26, no. 1, pp. 1–30, Dec. 1944.

[14] K. McQuade, J. Borstad, and A. de Oliveira, "Critical and theoretical perspective on scapular stabilization: What does it really mean, and are we on the right track?" *Phys. Therapy*, vol. 96, no. 8, pp. 1162–1169, Aug. 2016.

[15] M. L. Voight and B. C. Thomson, "The role of the scapula in the rehabilitation of shoulder injuries," *J. Athletic Training*, vol. 35, no. 3, pp. 364–372, 2000.

[16] A. Niyetkaliyev, E. Sariyildiz, and G. Alici, "Kinematic modelling and analysis of a novel bio-inspired and cable-driven hybrid shoulder mechanism," *J. Mech. Robot.*, vol. 13, no. 1, pp. 1–33, 2020.

[17] S. Christensen and S. Bai, "Kinematic analysis and design of a novel shoulder exoskeleton using a double parallelogram linkage," *J. Mech. Robot.*, vol. 10, no. 4, pp. 1–10, 2018.

[18] A. Q. L. Keemink, G. van Oort, M. Wessels, and A. H. A. Stienen, "Differential inverse kinematics of a redundant 4R exoskeleton shoulder joint," *IEEE Trans. Neural Syst. Rehabil. Eng.*, vol. 26, no. 4, pp. 817–829, Apr. 2018.

[19] H.-C. Hsieh, D.-F. Chen, L. Chien, and C.-C. Lan, "Design of a parallel actuated exoskeleton for adaptive and safe robotic shoulder rehabilitation," *IEEE/ASME Trans. Mechatronics*, vol. 22, no. 5, pp. 2034–2045, Oct. 2017.

[20] A. Zeiaee, R. Soltani-Zarrin, R. Langari, and R. Tafreshi, "Design and kinematic analysis of a novel upper limb exoskeleton for rehabilitation of stroke patients," in *Proc. Int. Conf. Rehabil. Robot. (ICORR)*, Jul. 2017, pp. 759–764.

[21] J. Hunt, H. Lee, and P. Artemiadis, "A novel shoulder exoskeleton robot using parallel actuation and a passive slip interface," *J. Mech. Robot.*, vol. 9, no. 1, pp. 1–7, 2017.

[22] R. John Varghese, G. Mukherjee, R. King, S. Keller, and A. D. Deshpande, "Designing variable stiffness profiles to optimize the physical human robot interface of hand exoskeletons," in *Proc. 7th IEEE Int. Conf. Biomed. Robot. Biomech. (Biorob)*, Aug. 2018, pp. 1101–1108.

[23] B. Kim and A. D. Deshpande, "An upper-body rehabilitation exoskeleton harmony with an anatomical shoulder mechanism: Design, modeling, control, and performance evaluation," *Int. J. Robot. Res.*, vol. 36, no. 4, pp. 414–435, 2017.

[24] B. Kim and A. D. Deshpande, "Controls for the shoulder mechanism of an upper-body exoskeleton for promoting scapulohumeral rhythm," in *Proc. IEEE Int. Conf. Rehabil. Robot. (ICORR)*, Aug. 2015, pp. 538–542.

[25] M. F. Levin, "Interjoint coordination during pointing movements is disrupted in spastic hemiparesis," *Brain*, vol. 119, no. 1, pp. 281–293, 1996.

[26] G. Wu *et al.*, "ISB recommendation on definitions of joint coordinate systems of various joints for the reporting of human joint motion—Part II: Shoulder, elbow, wrist and hand," *J. Biomech.*, vol. 38, no. 5, pp. 981–992, May 2005.

[27] R. M. Ehrig, W. R. Taylor, G. N. Duda, and M. O. Heller, "A survey of formal methods for determining the centre of rotation of ball joints," *J. Biomech.*, vol. 39, no. 15, pp. 2798–2809, Jan. 2006.

[28] M. Spong and M. Vidyasagar, *Robot Dynamics and Control*. New York, NY, USA: Wiley, 1989.

[29] J. van Kordelaar, E. E. H. van Wegen, and G. Kwakkel, "Unraveling the interaction between pathological upper limb synergies and compensatory trunk movements during reach-to-grasp after stroke: A cross-sectional study," *Exp. Brain Res.*, vol. 221, no. 3, pp. 251–262, Sep. 2012.

[30] J. M. Bland and D. Altman, "Statistical methods for assessing agreement between two methods of clinical measurement," *Lancet*, vol. 327, no. 8476, pp. 307–310, Feb. 1986.

[31] J. Bakdash and L. Marusich, "Repeated measures correlation," *SSRN Electron. J.*, vol. 8, pp. 1–13, Mar. 2017.

[32] B. Bouvier, S. Duprey, L. Claudon, R. Dumas, and A. Savescu, "Upper limb kinematics using inertial and magnetic sensors: Comparison of sensor-to-segment calibrations," *Sensors*, vol. 15, no. 8, pp. 18813–18833, Jul. 2015.

[33] A. Ferrari, A. G. Cutti, and A. Cappello, "A new formulation of the coefficient of multiple correlation to assess the similarity of waveforms measured synchronously by different motion analysis protocols," *Gait Posture*, vol. 31, no. 4, pp. 540–542, Apr. 2010.

[34] P. Garofalo *et al.*, "Inter-operator reliability and prediction bands of a novel protocol to measure the coordinated movements of shoulder-girdle and humerus in clinical settings," *Med. Biol. Eng. Comput.*, vol. 47, no. 5, pp. 475–486, May 2009.

[35] M. M. Mukaka, "Statistics corner: A guide to appropriate use of correlation coefficient in medical research," *Malawi Med. J.*, vol. 24, no. 3, pp. 69–71, Sep. 2012.

[36] P. M. Nair, T. G. Hornby, and A. L. Behrman, "Minimal detectable change for spatial and temporal measurements of gait after incomplete spinal cord injury," *Topics Spinal Cord Injury Rehabil.*, vol. 18, no. 3, pp. 273–281, Jul. 2012.

[37] J. M. Bland and D. G. Altman, "Measuring agreement in method comparison studies," *Stat. Methods Med. Res.*, vol. 8, no. 2, pp. 135–160, Jun. 1999.

[38] A. G. Cutti, G. Paolini, M. Troncossi, A. Cappello, and A. Davalli, "Soft tissue artefact assessment in humeral axial rotation," *Gait Posture*, vol. 21, no. 3, pp. 341–349, Apr. 2005.

[39] E. Todorov, "Probabilistic inference of multijoint movements, skeletal parameters and marker attachments from diverse motion capture data," *IEEE Trans. Biomed. Eng.*, vol. 54, no. 11, pp. 1927–1939, Nov. 2007.

[40] S. F. van Rijn, E. L. Zwerus, K. L. Koenraadt, W. C. Jacobs, M. P. van den Bekerom, and D. Eygendaal, "The reliability and validity of goniometric elbow measurements in adults: A systematic review of the literature," *Shoulder Elbow*, vol. 10, no. 4, pp. 274–284, Oct. 2018.

[41] M. J. Mullaney, M. P. McHugh, C. P. Johnson, and T. F. Tyler, "Reliability of shoulder range of motion comparing a goniometer to a digital level," *Physiotherapy Theory Pract.*, vol. 26, no. 5, pp. 327–333, Jul. 2010.

[42] F. Grimm, J. Kraugmann, G. Naros, and A. Gharabaghi. (2020). *Clinical Validation of Kinematic Assessments of Post-Stroke Upper Limb Movements With a Multi-Joint Arm Exoskeleton*. [Online]. Available: https://www.researchsquare.com/article/rs-52210/v1

[43] C. G. Rose, E. Pezent, C. K. Kann, A. D. Deshpande, and M. K. O'Malley, "Assessing wrist movement with robotic devices," *IEEE Trans. Neural Syst. Rehabil. Eng.*, vol. 26, no. 8, pp. 1585–1595, Aug. 2018.